Geosci. Model Dev. Discuss., 6, 4243–4280, 2013
www.geosci-model-dev-discuss.net/6/4243/2013/
doi:10.5194/gmdd-6-4243-2013
© Author(s) 2013. CC Attribution 3.0 License.

Geoscientific Model Development Discussions
Open Access

This discussion paper is/has been under review for the journal Geoscientific Model Development (GMD). Please refer to the corresponding final paper in GMD if available.

Optimization of a prognostic biosphere model in atmospheric CO_2 variability and terrestrial biomass

M. Saito[1,2], A. Ito[1], and S. Maksyutov[1]

[1]Center for Global Environmental Research, National Institute for Environmental Studies, Tsukuba, Japan
[2]Laboratoire des Sciences du Climat et de l'Environnement, UMR8212, CEA-CNRS-UVSQ, 91191 Gif sur Yvette, France

Received: 5 July 2013 – Accepted: 30 July 2013 – Published: 6 August 2013

Correspondence to: M. Saito (saito.makoto@nies.go.jp)

Published by Copernicus Publications on behalf of the European Geosciences Union.

Abstract

This study investigated the capacity of a prognostic biosphere model to simulate global vegetation carbon dynamics and the variability in atmospheric CO_2 concentrations under the current environmental conditions. Global data sets of atmospheric CO_2 concentrations and terrestrial vegetation compositions of the aboveground biomass and net primary productivity (NPP) were assimilated into the biosphere model using an inverse modeling method combined with an atmospheric transport model. In this process, the optimal physiological parameters of the biosphere model were estimated by minimizing the misfit between the observed and modeled values, and acceptable parameters with various values were generated among the biome types. The model with the optimized parameters corresponded to the observed seasonal variations in the CO_2 concentration, especially in the Northern Hemisphere where there are abundant observation stations, although the annual amplitudes were overestimated at a few stations. In simulating the mean annual aboveground biomass and NPP, the model also produced moderate estimates of the mean magnitudes and probability distributions for each biome. However, the model worked less efficiently in simulating the terrestrial vegetation compositions in some grids. These misfits suggest that some additional information about the disturbance and seasonal variability of the physiological parameters is required to improve the performance of the simulation model.

1 Introduction

The terrestrial biosphere generally absorbs CO_2 from the atmosphere, and its global carbon uptake rate is considered to be similar to that of the ocean (Tans et al., 1990). Many studies have tried to accurately quantify the total exchange rate between the terrestrial biosphere and the atmosphere, and to determine the role of the terrestrial biosphere in the global carbon cycle (e.g., Schimel, 1995; Field et al., 1998). Modeling the terrestrial biosphere is one of the key strategies used in these studies (e.g.,

GMDD
6, 4243–4280, 2013

Potter et al., 1993; Running and Hunt, 1993; Ito and Oikawa, 2002). Both diagnostic and prognostic biosphere models can simulate the main processes of plant physiology and carbon dynamics under given static climatic conditions. Dynamic global vegetation models have also recently attracted considerable attention (e.g., Sitch et al., 2003; Krinner et al., 2005; Sato et al., 2007).

However, each biosphere model uses individual approaches and representations to predict the important processes of the carbon dynamics in ecosystems. Therefore, the quantities in the carbon budgets derived from these models differ. Cramer et al. (1999) compared 17 biosphere models, and found that the global terrestrial net primary productivity (NPP) calculated with them ranged from about 40 to 65 $\mathrm{Pg\,C\,yr^{-1}}$, with different spatial distributions. Even at the regional scale, Ichii et al. (2010) reported large differences in the annual amounts of gross primary productivity (GPP) and ecosystem respiration among nine models when each original parameter set was used for the simulation. The discrepancies evident among these models when they are compared systematically indicate that current biosphere models still require improvement (Friedlingstein et al., 2006; Jung et al., 2007; Sitch et al., 2008).

Model–data synthesis is one approach to dealing with the problem discussed above, because it reduces the uncertainties and optimizes the controlling processes in the model to improve its fit to the observed data. This method is widely applied in terrestrial biosphere modeling, as in atmospheric and oceanic modeling, with various a priori information. Examples include the estimation of the residence times of carbon pools in soils and plants in regional areas (Barrett, 2002; Zhou and Luo, 2008), the fit of the models of eddy covariance flux variables at the point scale (Braswell et al., 2005; Sacks et al., 2006), the impact of seasonal water stress on ecosystem gas exchange (Reichstein et al., 2003), and atmospheric inversion schemes (Ciais et al., 1995; Enting et al., 1995; Bousquet et al., 2000; Peylin et al., 2005). An overview of model–data synthesis methods in terrestrial carbon studies and the improvements required are discussed in several studies (Raupach et al., 2005; Wang et al., 2009; Luo et al., 2011).

GMDD
6, 4243–4280, 2013

Using these model–data synthesis approaches, the study of Kaminski et al. (2002) introduced an important method with which to systematically infer optimal model parameters. The authors demonstrated the assimilation of observed atmospheric CO_2 concentrations into a terrestrial biosphere model by combining it with an atmospheric transport model. The atmospheric CO_2 concentration reflects the distributions of CO_2 sources and sinks at various spatial and temporal scales, rather than those restricted to a small spatial footprint, so these data are likely to be a suitable source of information with which to optimize a global biosphere model. In these studies, two parameters, light-use efficiency (LUE) and the sensitivity of respiration to temperature changes (Q_{10}) were individually modified for 12 biomes, which led the a good simulation of the general phase and amplitude of the seasonal cycles of atmospheric CO_2 at the observation sites. Rayner et al. (2005) further developed the study of Kaminski et al. (2002) by replacing the biosphere model with a more mechanistic one and optimizing many more model parameters, in what is known as the "Carbon Cycle Data Assimilation System" (CCDAS). The scheme for the uncertainty estimates in the simulation of CCDAS is also minutely discussed by Scholze et al. (2007).

These studies have focused predominantly on the CO_2 fluxes associated with atmospheric CO_2 variability, and less effort has been directed toward the effects of the optimized parameters on the variability in the ecosystem carbon pools or in plant material. However, the importance of estimating the forest carbon stock, as well as atmospheric CO_2 variability, is increasingly recognized in scientific and political circles (e.g., Carvalhais et al., 2010; Saatchi et al., 2011). This is because we must be confident of our estimates of the forest carbon stock to quantify the CO_2 emissions attributable to deforestation and forest degradation, which account for about 12 % or more of total anthropogenic CO_2 emissions (van der Werf et al., 2009). Improving the estimates of forest carbon stocks in parallel with those of atmospheric CO_2 variability is necessary to assess the global carbon balance and the role of the terrestrial biosphere in the current climate.

GMDD
6, 4243–4280, 2013

Here, we have developed an optimization scheme for a global biosphere model for atmospheric CO_2, aboveground biomass, and NPP data, combined with an atmospheric transport model and a Bayesian inversion method. Our primary goal was to improve the present assessments of the terrestrial carbon cycle under current climatic conditions and the interactions between the atmosphere and biosphere. For this purpose, we have focused on constructing a model that is capable of comprehensively simulating the carbon dynamics of natural vegetation, vegetation structure, and atmospheric CO_2 variability on a global scale.

2 Method and data

2.1 Terrestrial biosphere model

A prognostic biosphere model, the Vegetation Integrative SImulator for Trace gases (VISIT; Ito, 2010) was used to simulate the global terrestrial carbon cycle in this study. All variables in VISIT are calculated at a $2.5^{\circ} \times 2.5^{\circ}$ spatial resolution with a daily temporal step. The global vegetation types in the model are classified into 15 biomes (Fig. 1), and a map of their distributions was produced using the MODIS land cover data (Friedl et al., 2002). The reanalysis/assimilation data sets released by the Japan Meteorological Agency (JMA) and the Japan 25 yr reanalysis (JRA-25)/JMA Climate Data Assimilation System (JCDAS) (Onogi et al., 2007) were used for forcing in VISIT. JRA-25 covers the period from 1979 to 2004, and JCDAS covers the period after 2004. The meteorological data used to operate VISIT were downward shortwave radiation, total cloudiness, air temperature, ground surface temperature, soil temperatures, specific humidity, precipitation, and wind velocity. The precipitation bias in JRA-25/JCDAS was corrected based on the study of Saito et al. (2011). We used the climate data for the 31 yr period from 1979 to 2009 for both spin-up and model simulation. In the spin-up the 31 yr climate data were repeated over about 2000 yr until carbon pools reaching equilibrium state.

GMDD
6, 4243–4280, 2013

In the model, plant physiology and the carbon budget were simulated in each grid cell. Net ecosystem productivity (NEP) was defined as follows:

$$\mathrm{NEP} = \mathrm{NPP} - \mathrm{HR} = -\mathrm{NEE} \tag{1}$$

$$\mathrm{NPP} = \mathrm{GPP} - \mathrm{AR} \tag{2}$$

where HR is the heterotrophic respiration and AR is the autotrophic respiration. Daily GPP rate is expressed using the dry-matter production theory by Monsi and Saeki (1953):

$$\begin{aligned}\mathrm{GPP} &= \epsilon \int_0^{\mathrm{DL}} \int_0^{\mathrm{LAI}} P_\mathrm{c}\,\mathrm{d}\,\mathrm{LAI}\,\mathrm{d}t \\ &= \frac{2\epsilon P_\mathrm{sat}\mathrm{DL}}{K_\mathrm{a}} \left[\ln\left\{ 1 + \sqrt{1 + \frac{K_\mathrm{a} \cdot Q_\mathrm{e} \cdot \mathrm{PPFD}_\mathrm{mid}}{P_\mathrm{sat}}} \right\} \right. \\ &\quad \left. - \ln\left\{ 1 + \sqrt{1 + \frac{K_\mathrm{a} \cdot Q_\mathrm{e} \cdot \mathrm{PPFD}_\mathrm{mid} \cdot \exp(-K_\mathrm{a} \cdot \mathrm{LAI})}{P_\mathrm{sat}}} \right\} \right]\end{aligned} \tag{3}$$

where ϵ ($= 4.32 \times 10^{-4}$) is a unit converter from $\mu\mathrm{mol\,CO_2\,m^{-2}\,s^{-1}}$ to $\mathrm{Mg\,C\,ha^{-1}\,day^{-1}}$, DL is day length (h), LAI is leaf area index that is estimated as a function of the given specific leaf area, P_c is the single-leaf photosynthetic rate ($\mu\mathrm{mol\,CO_2\,m^{-2}}$), P_sat is the single-leaf photosynthetic rate under light saturation ($\mu\mathrm{mol\,CO_2\,m^{-2}}$), K_a is a function of solar height in dimensionless, Q_e is light-use efficiency ($\mathrm{mol\,CO_2\,mol^{-1}}$ photon), $\mathrm{PPFD_{mid}}$ is photosynthetic photon flux density (PPFD; $\mu\mathrm{mol\,photon\,m^{-1}\,S^{-1}}$) at the top canopy at mid day. $\mathrm{PPFD_{mid}}$ is estimated from the equation of Kuroiwa (1966) with including cloudy decline effect. Seasonal variations in P_sat are assumed to be dependent on the ground surface temperature (T_g; °C), intercellular $\mathrm{CO_2}$ concentration (C_i;

GMDD
6, 4243–4280, 2013

ppmv) that is estimated from ambient CO_2 concentration, and soil moisture (Φ; mm), as follows,

$$P_{sat} = P_{max} \cdot F_{tmp}(T_g) \cdot F_{stl}(C_i) \cdot F_{nstl}(\Phi) \quad (4)$$

where P_{max} is the potential maximum value of P_{sat} and F is the coefficient function used to calculate seasonal variations in P_{sat}. F_{tmp} is formulated using the maximum, minimum, and optimum temperatures (T_{max}, T_{min}, and T_{opt}, respectively) for photosynthesis, whereas F_{stl} and F_{nstl} are formulated using the photosynthesis-limiting factors for intercellular CO_2 concentration (kmci) and soil moisture (km_nstl).

$$F_{tmp} = \max\left[\min\left[\frac{(T_g - T_{max})(T_g - T_{min})}{(T_g - T_{max})(T_g - T_{min}) - (T_g - T_{opt})^2}, 1\right], 0\right] \quad (5)$$

$$F_{stl} = \max\left[\min\left[(1 - C_{stl}) + \frac{C_{stl} \cdot (C_i - CD_{cmp})}{\mathrm{kmci} + C_i}, 1\right], 0\right] \quad (6)$$

$$F_{nstl} = \max\left[\min\left[(1 - C_{sntl}) + \frac{C_{nstl} \cdot \Phi}{\Phi + FP_{sw} \cdot \mathrm{km\_nstl}}, 1\right], 0\right] \quad (7)$$

where CD_{cmp} is CO_2 compensation point (Brooks and Farquhar, 1985), FP_{sw} is soil water holding capacity (mm) that is give from soil property data, and C_{stl} and C_{nstl} are constant coefficients.

AR is the integration of both the growth and maintenance respiration from the foliage, stem and branch, and root components. The growth respiration (AR_G) of each component is the cost to produce new biomass, given as

$$AR_{GX} = rg_X \cdot TP_X \quad (8)$$

where rg_X is the specific growth respiration rate, TP_X is the carbon translocation rate, and the subscript $_X$ represents each component: foliage ($_{FL}$), stem and branch ($_{SB}$), and

GMDD
6, 4243–4280, 2013

root ($_{RT}$). In contrast, the maintenance respiration (AR_M) is represented as a function of T_g:

$$AR_{MX} = rm_X \cdot \exp\left[\frac{\ln Q_{10}}{10}(T_g - 15)\right] \cdot M_X \quad (9)$$

where rm_X is the specific maintenance respiration rate and M_X is the carbon mass for each component.

HR is the respiration from two layers: the litter (HR_L) and humus (HR_H). Both HR_L and HR_H are calculated as functions of the soil temperature at two depths, 10 cm (T_{s10}) and 200 cm (T_{s200}), and Φ in the upper and lower soil layers:

$$HR_L = shl \cdot M_L \cdot F_{HRL}(T_{s10}) \cdot F_{HRL}(\Phi_u) \quad (10)$$

$$HR_M = shm \cdot M_H \cdot F_{HRM}(T_{s200}) \cdot F_{HRL}(\Phi_l) \quad (11)$$

where shl and shm are the specific heterotrophic respiration rates and M_L and M_H are the carbon masses of the organic matter in the litter and humus layers, respectively. The annual mean value of T_{s10} was used as substitute for T_{s200} because JRA-25/JCDAS provides the soil temperature at depth.

In VISIT, the amount of litter fall (LF) is assumed to be proportional to the carbon mass of each component (foliage, stem and branch, and root) as:

$$LF_X = lf_X \cdot M_X \quad (12)$$

where lf_X is the specific litter fall rate.

In this study, we used prior parameters with the same values for all biome types (Table 1). The posterior parameter was estimated using Bayesian inversion. We selected the parameters being sensitive to NEE, NPP and biomass in sensitivity analysis, P_{max}, T_{min}, T_{opt}, km_nstl, rg_{FL}, rg_{RT}, rm_{FL}, rm_{RT}, Q_{10}, lf_{FL}, lf_{SB}, shl, and shm to optimize the fit of the model simulations to the observations (Table 1).

GMDD
6, 4243–4280, 2013

2.2 Atmospheric tracer transport model

The seasonal variability in the atmospheric CO_2 concentration at the observation sites was simulated using the National Institute for Environmental Studies/Frontier Research Center for Global Change (NIES/FRCGC) off-line global atmospheric tracer transport model (NIES-TM; Maksyutov et al., 2008). NIES-TM is one of the transport models evaluated in the Atmospheric Transport Model Intercomparison Project (TransCom; Law et al., 1996; Gurney et al., 2002). The vertical turbulent diffusion in the boundary layer of NIES-TM is parameterized using the monthly mean planetary boundary layer (PBL) heights derived from a three-hourly PBL height data set (Schubert et al., 1993).

We operated NIES-TM with a $2.5^\circ \times 2.5^\circ$ grid resolution and nine vertical levels, with forcing data from JRA-25/JCDAS. The oceanic CO_2 flux, fossil fuel emission inventory, and NEE in the terrestrial biosphere are required as a priori information to run NIES-TM. In this study, the ocean flux was derived from the Offline Ocean Tracer Transport Model (OTTM; Valsala and Maksyutov, 2010), and the emission data were from the Open-source Data Inventory of Anthropogenic CO_2 emission (ODIAC; Oda and Maksyutov, 2011). We ran NIES-TM for the most recent five-year period for which all the a priori information was available (2003–2007). The data for the first year were used for the spin-up, and the average value over the years 2004 and 2007 were used in the analysis. As shown by Gurney et al. (2004), there are uncertainties in atmospheric transport models, which result in discrepancies in the concentration distributions of the model. However, this problem was beyond the scope of our analysis, and we did not address the uncertainties in the concentrations derived from the NIES-TM simulation.

2.3 Bayesian inversion

We optimized a set of biophysical parameters in VISIT against the mean monthly atmospheric CO_2 and the mean annual amounts of NPP and aboveground biomass (AGB). In this study, we did not analyze the belowground processes because the availability of carbon stock information was restricted. The atmospheric transport model is a linear

GMDD
6, 4243–4280, 2013

function and atmospheric CO_2 can be expressed by multiplication with a nonlinear terrestrial biosphere model. To derive an optimal parameter set $\mathbf{m}$, the deviations of the model estimates from the observed data are minimized using a Bayesian inversion scheme. When the probability distributions of all the observed and a priori information on the biophysical parameters are assumed to be Gaussian, and their means are $\mathbf{d}_{obs}$ and $\mathbf{m}_p$, respectively, the misfit between $\mathbf{d}_{obs}$ and the modeled values $\mathbf{G}(\mathbf{m})$ for atmospheric CO_2, NPP, and AGB is defined by a cost function (Tarantola, 2005):

$$S(\mathbf{m}) = \frac{1}{2}\left[(\mathbf{G}(\mathbf{m}) - \mathbf{d}_{obs})^T \mathbf{C}_D^{-1} (\mathbf{G}(\mathbf{m}) - \mathbf{d}_{obs}) + (\mathbf{m} - \mathbf{m}_p)^T \mathbf{C}_M^{-1} (\mathbf{m} - \mathbf{m}_p)\right] \quad (13)$$

where superscript T denotes transpose, and $\mathbf{C}_D$ and $\mathbf{C}_M$ are the covariance matrices defining the uncertainties for $\mathbf{d}_{obs}$ and $\mathbf{m}_p$, respectively. This study fixed $\mathbf{C}_M$ at 10 % around each $\mathbf{m}_p$, and at 2 °C for T_{opt} and T_{min}. The values of $\mathbf{C}_D$ are described in the following section. The center of the posterior Gaussian distribution, which shows the optimized values for the model parameter $\mathbf{m}$, can be expressed following Tarantola (2005) as:

$$\mathbf{m} = \mathbf{m}_p + \left(\mathbf{G}^T \mathbf{C}_D^{-1} \mathbf{G} + \mathbf{C}_M^{-1}\right)^{-1} \mathbf{G}^T \mathbf{C}_D^{-1} (\mathbf{d}_{obs} - \mathbf{G}(\mathbf{m}_p)) \quad (14)$$

In this study, we inverted $\left(\mathbf{G}^T \mathbf{C}_D^{-1} \mathbf{G} + \mathbf{C}_M^{-1}\right)^{-1}$ in Eq. (14) using single-value decomposition.

The optimal parameter set $\mathbf{m}$ is given by minimizing $S(\mathbf{m})$. We used an iterative process to calculate the derivative of S for this minimization. The derivative is computed from the rate of change in S with respect to the small change in each target parameter around $\mathbf{m}_p$. The minimization of S was assessed by calculating χ^2, which is the mean square mismatch between $\mathbf{d}_{obs}$ and $\mathbf{G}(\mathbf{m})$. If the fits are good, $\chi^2 \approx 1$. A χ^2 value much larger than 1 indicates that the difference between the observation and prediction is much larger than the uncertainty used in the inversion.

GMDD
6, 4243–4280, 2013

2.4 Data

The monthly mean atmospheric CO_2 data from GLOBALVIEW-CO2 (2010) were used as the observation data for the CO_2 concentration. GLOBALVIEW-CO_2 is a product based on atmospheric measurements and provides information about CO_2 variability at over 100 sampling locations around the globe. The monthly mean CO_2 variability stored in the file named *statistical summary of the average seasonal pattern* (*seas*), which provides monthly mean values detrended by a smooth fit, was used in the following analysis. The standard error for *seas* each month was also used as a measure of the uncertainty in the observed CO_2 in $\mathbf{C}_D$ in Eqs. (13) and (14). In this study, we excluded all data sampled at locations in the ocean and some data sampled on islands from the analysis to reduce the contamination produced by uncertainties in the ocean flux. Consequently, we selected sampling locations at 74 sites, including 18 sites with multiple vertical CO_2 observations sampled by aircraft (Fig. 1). For those sites with a vertical profile, the partial column CO_2 concentrations were estimated from the vertical profiles by assuming that the CO_2 concentration at each observation height represents the concentration at altitudes centering round the observation height. We analyzed this partial column concentration instead of individual CO_2 concentrations at multiple heights.

The AGB data from the International Institute for Applied Systems Analysis (IIASA; Kindermann et al., 2008) were used in this study to optimize AGB of the biosphere model. IIASA provides half-degree global biomass and carbon stock data estimated with a downscaling model on the basis of a map provided by the Global Forest Resources Assessment. The data for AGB per hectare were calculated from the gridded AGB data divided by the grid area data. To reduce the discrepancies attributable to the differences in the dominant biome in each grid between the model and IIASA, the grid resolution for AGB was expanded to $7.5^\circ \times 7.5^\circ$. Therefore, the IIASA data with a grid resolution of $0.5^\circ \times 0.5^\circ$ and the VISIT data with a resolution of $2.5^\circ \times 2.5^\circ$ were aggregated to the desired resolution. Here, the mean AGB values in VISIT for the 10 yr

GMDD
6, 4243–4280, 2013

period 2000–2009 were used for the analysis. We compared AGB in 351 grids over the global terrestrial area.

The third data set contained the NPP data from the Global Primary Production Data Initiative (GPPDI; Scurlock et al., 1999; Olson et al., 2001). The GPPDI data set consists of three classes of NPP data: NPP measurements at intensively studied sites with site-specific information, NPP measurements at extensive sites with less-site-specific information, and gridded NPP data with a grid resolution of 0.5° compiled from collections of inventory, modeling, and remote sensing data. All these NPP data from the three classes were aggregated into a 7.5° grid cell, resulting in the 173 grids that were analyzed in this study. As for AGB, the NPP data in VISIT were averaged over the period 2000–2009 and were aggregated into 7.5° grid cells. The standard deviations in the calculation of the 7.5° grid mean values for AGB and NPP were used as the measures of data uncertainty $\mathbf{C}_D$ for each grid.

3 Results and Discussion

3.1 Model parameterization

The final value of χ^2 for the whole data in this study was 4.50; $\chi^2 = 0.98$ for atmospheric CO_2 and $\chi^2 = 9.80$ for AGB and NPP. These test statistics indicate that our optimization scheme fits the observed data less well for AGB and NPP than for atmospheric CO_2. This problem is discussed below.

The posterior parameters showed various changes from the prior parameters (Fig. 2). Here, we examine some parameters that show clear changes. Large increases and reductions in the magnitudes of the posterior parameters were observed for lf_{FL} and lf_{SB}. These parameters control the litter fall rate of the foliage and the stem and branch, respectively, which directly control the amount of biomass and indirectly affect the photosynthesis and respiration variability via changes in the LAI and carbon mass. The ratio of the litter production to the total organic matter of each component

GMDD
6, 4243–4280, 2013

increases with the value of lf, and vice versa. The deciduous needle-leaf forests, deciduous broad-leaf forests, and mixed forests have lower litter fall rates for stem and branch, whereas wooded grassland and closed shrubland have higher rates.

The P_{max} parameter, which defines the potential maximum photosynthetic rate, showed a slight decline from the prior magnitude for many biome types. Under natural conditions, P_{sat} shows large seasonal variations caused by temperature, water, and CO_2 conditions (Eq. 4), and the magnitudes and ranges of those variations were similar in most case to those reported in a previous study (Larcher, 2003).

At the site scale, the decline in the magnitude of Q_{10} with increasing temperature has been reported for various plants (e.g., Atkin et al., 2000; Tjoelker et al., 2001), indicating that the response of respiration to temperature becomes smaller at higher temperatures because of substrate limitations (Atkin and Tjoelker, 2003). This temperature dependence of Q_{10} was observed in the present study, with a large scatter ranging from 1.68 to 2.32, and a liner regression of $Q_{10} = -0.01T + 2.10$ ($r^2 = 0.46, P < 0.05$), where T is the temperature for 13 biomes, excluding wooded grassland and snow and ice (Fig. 3). This range in the variability of Q_{10} and the slope of the regression are substantially smaller than those reported in previous studies. These differences may be attributable to differences in the spatial and temporal scales analyzed. The posterior Q_{10} indicates the mean sensitivity over long-term and regional scales, and was fixed to one value for all biomes, regardless of their specific temperature ranges, whereas in previous studies, the Q_{10} measure represented short-term and individual points. However, in contrast to our study, which demonstrated the temperature dependence of Q_{10}, another recent study based on in situ data reported that the Q_{10} parameter, was independent of the mean annual temperature and was almost constant at around 1.4 ± 0.1 across biomes (Mahecha et al., 2010). From these results, it seems that there is still great uncertainty in the behavior of the posterior Q_{10}, so further research is required to clarify it.

There were no clear changes in the temperature parameters for photosynthesis, which were within $\pm 1\,^{\circ}C$ of the prior values for the optimum temperature T_{opt}, except for

GMDD
6, 4243–4280, 2013

the evergreen broad-leaf forests and grasslands; with slight changes in the minimum temperature T_{min}, within the range of −5.4–4.8 °C. Although T_{opt} describes the optimal season for photosynthesis, T_{min} mainly controls the phases of leafing and senescence and the length of photosynthetic activity. Therefore, T_{min} can be a sensitive parameter for improving the simulation of atmospheric CO_2 seasonality.

3.2 Atmospheric CO_2 simulation

Atmospheric CO_2 variability was estimated over the globe and the mean monthly concentrations were compared with the observed data from GLOBALVIEW-CO_2 at 74 stations. The results estimated from the posterior NEE showed good agreement with the observations for the large domain and seasonality ($r^2 = 0.84, P < 0.001$; Fig. 4). The slope of the linear regression indicated that the modeled CO_2 variability was slightly overestimated without offset. The annual mean χ^2 values at each station ranged from 0.02 to 6.39, and the annual mean values of the root mean square error (RMSE) varied from 0.50 to 4.82 ppm, with a mean RMSE of 0.99 ppm.

Figure 5 shows the mean seasonal variations in atmospheric CO_2 at the Cape Grim station, Tasmania, Australia (CGO; 40.68° S, 144.69° E) and Wendover station, Utah, USA (UTA; 39.90° N, 113.72° W), as examples. The biome types at CGO and UTA stations are classified as cropland and temperate open shrubland, respectively. The annual mean χ^2 and RMSE values for the observed and posterior data were 6.39 and 1.14 ppm, respectively, at CGO and 0.03 and 0.50 ppm, respectively, at UTA. CGO was the station with the largest annual mean χ^2 value among all the stations. The annual amplitude of the concentration at CGO is obviously overestimated. There was also a discrepancy in the phase of the seasonal variability between the observations and the model. Slight improvement can be seen in the results for the posterior parameter compared with the prior parameter, but the CO_2 variability is still outside the domain of the uncertainties in the observed data. Because the variability in CO_2 on an island is mainly controlled by the oceanic flux, the biosphere model is usually negligibly responsible for the errors in the CO_2 concentration (Rayner et al., 2005). However, we found

GMDD
6, 4243–4280, 2013

that the contribution of the terrestrial flux to the CO_2 concentration at the CGO station was much greater than that of the oceanic flux. The overestimation of the terrestrial flux is mainly attributed to the unsuccessful optimization of the biosphere model because there are limited observation stations in the Southern Hemisphere. Indeed, all the observation stations located in the cropland grid extend across Europe and the USA, except the CGO station (Fig. 1). The difficulties encountered in concentration modeling in regions with a sparse coverage of observation stations have also been discussed by Gurney et al. (2004). This result suggests that an increase in the observation stations in the terrestrial areas of the Southern Hemisphere is required to allow the more precise simulation of atmospheric CO_2 variability.

At the UTA station, the prior concentration showed overestimates of both the photosynthetic uptake in summer and the respiration release in winter of a few ppm (Fig. 5b). The posterior concentration reduced these to a difference of within a few tenths of a ppm. After the optimization of the biosphere model, four of the 74 stations had annual mean χ^2 values of > 3. Two of these stations were located in the Southern Hemisphere, CGO and the Syowa station, Antarctica (SYO: 69.00° S, 39.58° E; χ^2 = 3.86), and the other two were either on a cape, Cape Ochi-ishi, Japan (COI: 43.15° N, 145.50° E; χ^2 = 3.43), or in a highland region, Boulder Atmospheric Observatory, Colorado, USA (BAO: 40.05° N, 105.00° W; χ^2 = 4.63). The discrepancies at the latter two stations are probably attributable to the coarse horizontal resolution of our model. The atmospheric CO_2 variability at stations located in complex terrains is substantially influenced by local mesoscale motions, which lead to errors in the concentration simulations when a global model is used (Ahmadov et al., 2009).

Figure 6 shows a comparison of the mean seasonal amplitudes of atmospheric CO_2 based on the observed and posterior parameters at all stations along a single latitude. The seasonal amplitude at each station was defined as the difference between the maximum and minimum mean monthly concentrations. The posterior simulation showed an appropriate representation of the seasonal amplitude in the Northern Hemisphere, attributed to the large number of observation stations. The latitudinal

GMDD
6, 4243–4280, 2013

mean amplitude and its standard deviation for each 30° band from north to south were 15.4±1.6 (n = 8), 12.8±3.8 (n = 47), 7.7±0.7 (n = 5), 3.3±1.8 (n = 5), 1.0±0.4 (n = 3), and 1.1 ± 0.2 ppm (n = 6) for the observed data, and 16.9 ± 3.8, 12.6 ± 4.9, 7.1 ± 1.6, 3.2 ± 1.4, 3.5 ± 0.2, and 3.1 ± 0.4 ppm, respectively, for the posterior data. Erroneous overestimates were made at a few stations in the Northern Hemisphere, especially at Fraserdale station, Canada (FSD: 49.88° N, 81.57° W) and Pallas-Sammaltunturi GAW station, Finland (PAL: 67.97° N, 24.12° E). The seasonal variability in the posterior parameters at both stations showed overestimates of the winter concentration and the maximum photosynthetic uptake, which occurs in early summer. Unfortunately, in this study, we failed to improve these mismatches to produce good agreement with the observations at other stations. This is partly because of the inability of the global biosphere model to represent NEE variability in the areas around the observation points, and also because unsuitable biophysical parameters were selected for adjustment in the optimization process.

In contrast, the seasonal amplitudes of the posterior CO_2 concentration in the Southern Hemisphere tended to be about 2 ppm larger than the observed concentrations. As mentioned above, these larger ranges of amplitude are presumably attributable to the deficiency in observation stations and to some problems with transport errors and with the a priori sources in this region. We are currently trying to update the atmospheric transport model to reduce the uncertainty in it and to improve the model representations with higher spatial and temporal resolutions (Belikov et al., 2011).

3.3 Biomass simulations

The χ^2 values for AGB and NPP for the observed and posterior data ranged from 0.00 to 2249 among the grids, with a mean value of 9.80. Six of the total 589 grids with 7.5° × 7.5° resolution showed erroneous χ^2 values much larger than 100. In all these grids, the observed AGB and its uncertainty were approximately 0, but the posterior AGB had values ranged from 1.8 to 7.2 kgC m^{-2}, which resulted in an erroneously elevated χ^2 value. These larger values suggested that the uncertainty in the observed

GMDD
6, 4243–4280, 2013

data applied to these grids was too small, and there are some discrepancies in biome types between the observation and the model in the grids. If the χ^2 values for these six grids are excluded from the analysis, the mean χ^2 values for AGB and NPP decrease to 1.89.

The mean annual AGB and NPP values estimated with a spatial resolution of 2.5° × 2.5° using the posterior parameters were compared with IIASA and GPPDI data for each biome type (Table 2, Figs. 7 and 8). The IIASA data showed biome-specific patterns in the mean ABG. The biomes with AGB > 3 kg C m^{-2} and relatively large scatters were the evergreen broad-leaf forest (EBF), deciduous broad-leaf forest (DBF), and woodland (WL); those with AGB of about 2–3 kg C m^{-2} were the evergreen needle-leaf forest (ENF), deciduous needle-leaf forest (DNF), and mixed forest (MF); and the other biome types had AGB < 2 kg C m^{-2}. These biome patterns in mean AGB values and total AGB distributions are well represented in the simulation with the posterior parameters, except that AGB variability is underestimated in EBF. The AGB of EBF in IIASA ranged from 0.1 to 17.5 kg C m^{-2}, with lower and upper quartiles of 1.7 and 7.5 kg C m^{-2}, respectively, whereas that of the model ranged from 0.6 to 7.6 kg C m^{-2}, with lower and upper quartiles of 4.4 and 5.4 kg C m^{-2}, respectively. This slight variability in AGB is partly attributable to the small variability in NPP in GPPDI, which constrains large variations in AGB during parameter optimization. It is also probably attributable to the fact that the model does not consider the effects of land use changes, which could directly affect the AGB distribution (Achard et al., 2002).

The mean NPP for each biome type in the GPPDI distributions ranged from 300 to 600 g C m^{-2} yr^{-1}, except for the much higher NPP in EBF and the lower NPP in the tundra (TND), temperate open shrubland (TOS), and bare ground (BG). Although these biome-specific distributions of the mean NPP differ from those of AGB, the mean NPP and total NPP distribution for each biome type estimated from the posterior data matched the GPPDI observed data reasonably well. NPP is partly lost as litter and is partly grazed by consumers, and the rest is used to build up the plant biomass. In this study, although the impact of grazing loss was not considered in the model, the

GMDD
6, 4243–4280, 2013

relationship between NPP and ABG in the different biome types was mainly controlled by adjusting the litter fall rate parameter, which produced moderate fits to the observed mean annual AGB and NPP.

However, the model underestimated the mean annual NPP and its distribution in WGL, with an average value of $322 \pm 297\,\mathrm{g\,C\,m^{-2}\,yr^{-1}}$ compared with the observed value of $502 \pm 347\,\mathrm{g\,C\,m^{-2}\,yr^{-1}}$ (Table 2 and Fig. 8). The vegetation structure and carbon dynamics in WGL are under the control of fire disturbance (Grace et al., 2006), and in burnt areas, the emitted CO_2 is assimilated by the regrowing vegetation. Despite this, we did not consider the effect of fire disturbance in this study, because there are still uncertainties in modeling fire frequency and intensity and their contributions to the vegetation dynamics on the global scale over a long period (Thonicke et al., 2010), which is also true of the effects of land use changes and grazing. Further work is required to expand the model to simulate natural and anthropogenic disturbances and their impact on vegetation. The explicit difference between GPPDI and the model regarding NPP at BG was attributed to discrepancies in the biome type in the grids.

The biosphere model VISIT is designed to be used with biome-specific parameters that have constant values for each biome, and many of which are independent of environmental influences. The parameters optimized in this study, such as the specific growth respiration (rg_X) and litter fall (lf_X) rates, have constant values for each biome (Eqs. 8 and 12), indicating that these parameters have been adjusted to especially represent the central parts of the distributions of the corresponding physiological processes. However, for example, vegetation alters its biomass allocation patterns in response to differences in the climate to allow its survival under unfavorable conditions (Callaway et al., 1994; Maherali and DeLucia, 2001), and the amount of litter fall also varies considerably under different environmental conditions (Berg and Laskowski, 2006), and none of these factors are included in the model. Therefore, the model far from adequately represents the physiological processes under all conditions, which might result in large discrepancies from the observed data at some points. If it is possible to describe the the response of each parameter to the environmental conditions,

GMDD
6, 4243–4280, 2013

a model that includes those variable parameters could improve the simulation of global carbon sequestration and its distribution, although adopting empirical rules entails the possibility that the uncertainties in the modeling will increase (Saito et al., 2009).

In this study, we selected 13 key parameters in a prognostic biosphere model for model–data synthesis by trial and error. Caution is required because it might be possible to obtain similar model results with different combinations of model parameters (Wang et al., 2009). For example, the specific leaf area (SLA) is strongly linked to the photosynthetic capacity and the leaf lifespan (Wright et al., 2004), and indeed SLA does show similar effects to those of P_{max} and lf_{FL} on the model photosynthetic uptake rate. Nevertheless, the parameter SLA was eliminated from the analysis because there are insufficient observation data to distinguish the corresponding optimal parameter values from the three mutually correlated parameters. Therefore, additional observations would be useful in optimizing many more model parameters and enhancing the performance of the model–data synthesis.

3.4 Global carbon exchanges

The mean global carbon fluxes estimated from the posterior parameters were a GPP of 112.5 $PgCyr^{-1}$, NPP of 52.7 $PgCyr^{-1}$, NEP of 2.0 $PgCyr^{-1}$, AR_G of 20.6 $PgCyr^{-1}$, AR_M of 40.2 $PgCyr^{-1}$, and HR of 49.8 $PgCyr^{-1}$. These total fluxes can be compared with the corresponding mean values of Rayner et al. (2005): 134.8, 40.6, 2.5, 22.4, and 72.7 $PgCyr^{-1}$ for GPP, NPP, NEP, AR_G, and AR_M, respectively, in the period 1980–2000. The mean result for AR_G in this study was similar to the values in that study, but AR_M was about 30 $PgCyr^{-1}$ smaller than in that study. The ratio of AR_M to autotrophic respiration varies between 25 % and 90 %, according to with plant size (van Iersel, 2003), and the global mean value in this study was 66 %. A large part of the difference in AR_M is compensated by the difference in GPP. The global GPP in this study was also smaller than the value of Krinner et al. (2005) of 137.4 $PgCyr^{-1}$, but was similar to the value of Zhao et al. (2005) of 109.3 $PgCyr^{-1}$. The total NPP was within the range of

GMDD
6, 4243–4280, 2013

$56.2 \pm 14.3\,\mathrm{Pg\,C\,yr^{-1}}$ according to a metaanalysis of global NPP (Ito, 2011), and was between the lower quartile and the median values of the global NPP distribution of 251 estimates. The mean NEP had a similar value to those of other studies, including model estimates (Cramer et al., 2001; Le Quéré et al., 2009) and analysis of the atmospheric O_2/N_2 ratio (Keeling et al., 1996). These estimates of global carbon fluxes are overall consistent with those of previous studies. Therefore, the model used with posterior parameters could be valuable in analyzing current global vegetation carbon dynamics, and it should be possible to apply it to the prediction of these dynamics under changed environmental conditions.

4 Conclusions

This study has described a framework for the optimization of a prognostic biosphere model and some typical results estimated from the posterior parameters. We used a Bayesian inversion method to improve the model estimates against the observed variability in atmospheric CO_2 concentrations, the mean annual aboveground biomass, and NPP by adjusting the physiological model parameters. The litter fall rate parameter was important in calculating the balance between the atmospheric CO_2 and biomass, because it directly controls the vegetation biomass and indirectly affects the photosynthetic uptake and respiration release rates. The minimum temperature for photosynthesis is also a significant parameter in simulating phenological phenomena. The model used with posterior parameters produced moderate seasonal variations in atmospheric CO_2 and the distributions of the mean amounts of aboveground biomass and NPP, suggesting that the model could be useful in understanding the dynamics of the global carbon cycle. However, it must be noted that the following are all important requirements if we are to improve carbon cycle modeling: more observations and improvements in the model regarding the physiological processes and global biome distributions; reductions in the uncertainties in the atmospheric transport model and the a priori information; and models with greater spatial and temporal resolution.

GMDD
6, 4243–4280, 2013

The publication of this article
is financed by CNRS-INSU.

References

Achard, F., Eva, H. D., Stibig, H. J., Mayaux, P., Gallego, J., Richards, T., and Malingreau, J. P.: Determination of deforestation rates of the world's humid tropical forests, Science, 297, 999–1002, 2002. 4259

Ahmadov, R., Gerbig, C., Kretschmer, R., Körner, S., Rödenbeck, C., Bousquet, P., and Ramonet, M.: Comparing high resolution WRF-VPRM simulations and two global CO_2 transport models with coastal tower measurements of CO_2, Biogeosciences, 6, 807–817, doi:10.5194/bg-6-807-2009, 2009. 4257

Atkin, O. K. and Tjoelker, M. G.: Thermal acclimation and the dynamic response of plant respiration to temperature, Trends Plant Sci., 8, 343–351, 2003. 4255

Atkin, O. K., Holly, C., and Ball, M. C.: Acclimation of snow gum (*Eucalyptus pauciflora*) leaf respiration to seasonal and diurnal variations in temperature: the importance of changes in the capacity and temperature sensitivity of respiration, Plant Cell Environ., 23, 15–26, 2000. 4255

Barrett, D. J.: Steady state turnover time of carbon in the Australian terrestrial biosphere, Global Biogeochem. Cy., 16, 1108, doi:10.1029/2002GB001860, 2002. 4245

Belikov, D., Maksyutov, S., Miyasaka, T., Saeki, T., Zhuravlev, R., and Kiryushov, B.: Mass-conserving tracer transport modelling on a reduced latitude-longitude grid with NIES-TM, Geosci. Model Dev., 4, 207–222, doi:10.5194/gmd-4-207-2011, 2011. 4258

Berg, B. and Laskowski, R.: Litter decomposition: a guide to carbon and nutrient turnover, Adv. Ecol. Res., 38, 1–423, 2006. 4260

GMDD
6, 4243–4280, 2013

Bousquet, P., Peylin, P., Ciais, P., Le Quéré, C., Friedlingstein, P., and Tans, P. P.: Regional changes in carbon dioxide fluxes of land and oceans since 1980, Science, 290, 1342–1346, 2000. 4245

Braswell, B. H., Sacks, W. J., Linder, E., and Schimel, D. S.: Estimating diurnal to annual ecosystem parameters by synthesis of a carbon flux model with eddy covariance net ecosystem exchange observations, Glob. Change Biol., 11, 335–355, 2005. 4245

Brooks, A. and Farquhar, G. D.: Effect of temperature on the CO_2/O_2 specificity of ribulose-1,5-bisphosphate carboxylase/oxygenase and the rate of respiration in the light, Planta, 165, 397–406, 1985. 4249

Callaway, R. M., DeLucia, E. H., and Schlesinger, W. H.: Biomass allocation of montane and desert ponderosa pine: an analog for response to climate change, Ecology, 75, 1474–1481, 1994. 4260

Carvalhais, N., Reichstein, M., Ciais, P., Collatz, G. J., Mahecha, M. D., Montagnani, L., Papale, D., Rambal, S., and Seixas, J.: Identification of vegetation and soil carbon pools out of equilibrium in a process model via eddy covariance and biometric constraints, Glob. Change Biol., 16, 2813–2829, 2010. 4246

Ciais, P., Tans, P. P., Trolier, M., White, J. W. C., and Francey, R. J.: A large Northern Hemisphere terrestrial CO_2 sink indicated by the $^{13}C/^{12}C$ ratio of atmospheric CO_2, Science, 269, 1098–1102, 1995. 4245

Cramer, W., Kicklighter, D. W., Bondeau, A., Moor III, B., Churkina, G., Nemry, B., Ruimy, A., Schloss, A. L., and the participants of the Potsdam NPP Model intercomparison: Comparing global models of terrestrial net primary productivity (NPP): overview and key results, Glob. Change Biol., 5, 1–15, 1999. 4245

Cramer, W., Bondeau, A., Woodward, F. I., Prentice, I. C., Betts, R. A., Brovkin, V., Cox, P. M., Fisher, V., Foley, J. A., Friend, A. D., Kucharik, C., Lomas, M. R., Ramankutty, N., Sitch, S., Smith, B., White, A., and Young-Molling, C.: Global response of terrestrial ecosystem structure and function to CO_2 and climate change: results from six dynamic global vegetation models, Glob. Change Biol., 7, 357–373, 2001. 4262

Enting, I. G., Trudinger, C. M., and Francey, R. J.: A synthesis inversion of the concentration and $\delta^{13}C$ of atmospheric CO_2, Tellus, 47, 35–52, 1995. 4245

Field, C. B., Behrenfeld, M. J., Randerson, J. T., and Falkowski, P.: Primary production of the biosphere: integrating terrestrial and oceanic components, Science, 281, 237–240, 1998. 4244

GMDD
6, 4243–4280, 2013

Friedl, M. A., McIver, D. K., Hodges, J. C. F., Zhang, X. Y., Muchoney, D., Strahler, A. H., Woodcock, C. E., Gopal, S., Schneider, A., Cooper, A., Baccini, A., Gao, F., and Schaaf, C.: Global land cover mapping from MODIS: algorithms and early results, Remote Sens. Environ., 83, 287–302, 2002. 4247

Friedlingstein, P., Cox, P., Betts, R., Bopp, L., von Bloh, W., Brovkin, V., Cadule, P., Doney, S., Eby, M., Fung, I., Bala, G., John, J., Jones, C., Joos, F., Kato, T., Kawamiya, M., Knorr, W., Lindsay, K., Matthews, H. D., Raddatz, T., Rayner, P., Reick, C., Roeckner, E., Schnitzler, K.-G., Schnur, R., Strassmann, K., Weaver, A. J., Yoshikawa, C., and Zeng, N.: Climate–carbon cycle feedback analysis: results from the C4MIP model intercomparison, J. Climate, 19, 3337–3353, 2006. 4245

GLOBALVIEW-CO_2: Cooperative Atmospheric Data Integration Project–Carbon Dioxide, NOAA ESRL, 2010. 4253

Grace, J., José, J. S., Meir, P., Miranda, H. S., and Montes, R. A.: Productivity and carbon fluxes of tropical savannas, J. Biogeogr., 33, 387–400, 2006. 4260

Gurney, K. R., Law, R. M., Denning, A. S., Rayner, P. J., Baker, D., Bousquet, P., Bruhwiler, L., Chen, Y. H., Ciaisand, P., Fan, S., Fung, I. Y., Gloor, M., Heimann, M., Higuchi, K., John, J., Maki, T., Maksyutov, S., Masarie, K., Peylin, P., Prather, M., Pak, B. C., Randerson, J., Sarmiento, J., Taguchi, S., Takahashi, T., and Yuen, C. W.: Towards robust regional estimates of CO_2 sources and sinks using atmospheric transport models, Nature, 415, 626–630, 2002. 4251

Gurney, K. R., Law, R. M., Denning, A. S., Rayner, P. J., Pak, B. C., Baker, D., Bousquet, P., Bruhwiler, L., Chen, Y., Ciais, P., Fung, I. Y., Heimann, M., John, J., Maki, T., Maksyutov, S., Peylin, P., Prather, M., and Taguchi, S.: Transcom 3 inversion intercomparison: model mean results for the estimation of seasonal carbon sources and sinks, Global Biogeochem. Cy., 18, GB1010, doi:10.1029/2003GB002111, 2004. 4251, 4257

Ichii, K., Suzuki, T., Kato, T., Ito, A., Hajima, T., Ueyama, M., Sasai, T., Hirata, R., Saigusa, N., Ohtani, Y., and Takagi, K.: Multi-model analysis of terrestrial carbon cycles in Japan: limitations and implications of model calibration using eddy flux observations, Biogeosciences, 7, 2061–2080, doi:10.5194/bg-7-2061-2010, 2010. 4245

Ito, A.: Changing ecophysiological processes and carbon budget in East Asian ecosystems under near-future changes in climate: implications for long-term monitoring from a process-based model, J. Plant Res., 123, 577–588, 2010. 4247

GMDD
6, 4243–4280, 2013

Ito, A.: A historical meta-analysis of global terrestrial net primary productivity: are estimates converging?, Glob. Change Biol., 17, 3161–3175, 2011. 4262
Ito, A. and Oikawa, T.: A simulation model of the carbon cycle in land ecosystems (Sim-CYCLE): a description based on dry-matter production theory and plot-scale validation, Ecol. Model., 151, 143–176, 2002. 4245
Jung, M., Vetter, M., Herold, M., Churkina, G., Reichstein, M., Zaehle, S., Ciais, P., Viovy, N., Bondeau, A., Chen, Y., Trusilova, K., Feser, F., and Heimann, M.: Uncertainties of modeling gross primary productivity over Europe: a systematic study on the effects of using different drivers and terrestrial biosphere models, Global Biogeochem. Cy., 21, GB4021, doi:10.1029/2006GB002915, 2007. 4245
Kaminski, T., Knorr, W., Rayner, P. J., and Heimann, M.: Assimilating atmospheric data into a terrestrial biosphere model: a case study of the seasonal cycle, Global Biogeochem. Cy., 16, 1066, doi:10.1029/2001GB001463, 2002. 4246
Keeling, R. F., Piper, S. C., and Heimann, M.: Global and hemispheric CO_2 sinks deduced from changes in atmospheric O_2 concentration, Nature, 381, 218–221, 1996. 4262
Kindermann, G. E., McCallum, I., Fritz, S., and Obersteiner, M.: A global forest growing stock, biomass and carbon map based on FAO statistics, Silva Fenn., 42, 387–396, 2008. 4253
Krinner, G., Viovy, N., de Noblet–Ducoudré, N., Ogée, J., Polcher, J., Friedlingstein, P., Ciais, P., Sitch, S., and Prentice, I. C.: A dynamic global vegetation model for studies of the coupled atmosphere–biosphere system, Global Biogeochem. Cy., 19, GB1015, doi:10.1029/2003GB002199, 2005. 4245, 4261
Kuroiwa, S.: Dry matter production by plants, Modern Biology, 9, 71–100, 1966. 4248
Larcher, W.: Physiological Plant Ecology, Ecophysiology and Stress Physiology of Functional Groups, Springer, Berlin, Heidelberg, New York, 2003. 4255
Law, R. M., Rayner, P. J., Denning, A. S., Erickson, D., Fung, I. Y., Heimann, M., Piper, S. C., Ramonet, M., Taguchi, S., Taylor, J. A., Trudinger, C. M., and Watterson, I. G.: Variations in modeled atmospheric transport of carbon dioxide and the consequences for CO_2 inversions, Global Biogeochem. Cy., 10, 783–796, 1996. 4251
Le Quéré, C., Raupach, M. R., Canadell, J. G., Marland, G., Bopp, L., Ciais, P., Conway, T. J., Doney, S. C., Feely, R. A., Foster, P., Friedlingstein, P., Gurney, K., Houghton, R. A., House, J. I., Huntingford, C., Levy, P. E., Lomas, M. R., Majkut, J., Metzl, N., Ometto, J. P., Peters, G. P., Prentice, I. C., Randerson, J. T., Running, S. W., Sarmiento, J. L., Schuster, U.,

GMDD
6, 4243–4280, 2013

Sitch, S., Takahashi, T., Viovy, N., van der Werf, G. R., and Woodward, F. I.: Trends in the sources and sinks of carbon dioxide, Nat. Geosci., 2, 831–836, 2009. 4262
Luo, Y., Ogle, K., Tucker, C., Fei, S., Gao, C., LaDeau, S., Clark, J. S., and Schimel, D. S.: Ecological forecasting and data assimilation in a data-rich era, Ecol. Appl., 21, 1429–1442, 2011. 4245
Mahecha, M. D., Reichstein, M., Carvalhais, N., Lasslop, G., Lange, H., Seneviratne, S. I., Vargas, R., Ammann, C., Arain, M. A., Cescatti, A., Janssens, I. A., Migliavacca, M., Montagnani, L., and Richardson, A. D.: Global convergence in the temperature sensitivity of respiration at ecosystem level, Science, 329, 838–840, 2010. 4255
Maherali, H. and DeLucia, E. H.: Influence of climate-driven shifts in biomass allocation on water transport and storage in ponderosa pine, Oecologia, 129, 481–491, 2001. 4260
Maksyutov, S., Patra, P. K., Onishi, R., Saeki, T., and Nakazawa, T.: NIES/FRCGC Global Atmospheric Tracer Tnansport Model: description, validation, and surface sources and sinks inversion, J. Earth Sim., 9, 3–18, 2008. 4251
Monsi, M. and Saeki, T.: Über den Lichtfaktor in den Pflanzengesellschaften und seine Bedeutung für die Stoffproduktion, Jpn. J. Bot., 14, 22–52, 1953. 4248
Oda, T. and Maksyutov, S.: A very high-resolution (1 km × 1 km) global fossil fuel CO_2 emission inventory derived using a point source database and satellite observations of nighttime lights, Atmos. Chem. Phys., 11, 543–556, doi:10.5194/acp-11-543-2011, 2011. 4251
Olson, R. J., Johnson, K. R., Zheng, D. L., and Scurlock, J. M. O.: Global and Regional Ecosystem Modeling: Databases of Model Drivers and Validation Measurements, Ork Ridge National Laboratory, 2001. 4254
Onogi, K., Tsutsui, J., Koide, H., Sakamoto, M., Kobayashi, S., Hatsushika, H., Matsumoto, T., Yamazaki, N., Kamahori, H., Takahashi, K., Kadokura, S., Wada, K., Kato, K., Oyama, R., Ose, T., Mannoji, N., and Taira, R.: The JRA-25 reanalysis, J. Meteorol. Soc. Jpn., 85, 369–432, 2007. 4247
Peylin, P., Bousquet, P., Le Quéré, C., Sitch, S., Friedlingstein, P., McKinley, G., Gruber, N., Rayner, P., and Ciais, P.: Multiple constraints on regional CO_2 flux variations over land and oceans, Global Biogeochem. Cy., 19, GB1011, doi:10.1029/2003GB002214, 2005. 4245
Potter, C. S., Randerson, J. T., Field, C. B., Matson, P. A., Vitousek, P. M., Moonet, H. A., and Klooster, S. A.: Terrestrial ecosystem production: a process model based on global satellite and surface data, Global Biogeochem. Cy., 7, 811–841, 1993. 4245

GMDD
6, 4243–4280, 2013

Raupach, M. R., Rayner, P. J., Barrett, D. J., DeFries, R. S., Heimann, M., Ojima, D. S., Quegan, S., and Schmullius, C. C.: Model–data synthesis in terrestrial carbon observation: methods, data requirements and data uncertainty specifications, Glob. Change Biol., 11, 378–397, 2005. 4245

Rayner, P. J., Scholze, M., Knorr, W., Kaminski, T., Giering, R., and Widmann, H.: Two decades of terrestrial carbon fluxes from a carbon cycle data assimilation system (CCDAS), Global Biogeochem. Cy., 19, BG2026, doi:10.1029/2004GB002254, 2005. 4246, 4256, 4261

Reichstein, M., Tenhunen, J., Roupsard, O., Ourcival, J. M., Rambal, S., Miglietta, F., Peressotti, A., Pecchiari, M., Tirone, G., and Valentini, R.: Inverse modeling of seasonal drought effects on canopy CO_2/H_2O exchange in three Mediterranean ecosystems, J. Geophys. Res., 108, 4726, doi:10.1029/2003JD003430, 2003. 4245

Running, S. W. and Hunt, E. R.: Generalization of a forest ecosystem process model for other biomes, BIOME-BGC, and an application for global scale models, in: Scaling Physiological Processes: Leat to Globe, edited by: Ehleringer, J. R. and Field, C. B., Academic Press, 141–158, 1993. 4245

Saatchi, S. S., Harris, N. L., Brown, S., Lefsky, M., Mitchard, E. T. A., Salas, W., Zutta, B. R., Buermann, W., Lewis, S. L., Hagen, S., Petrova, S., White, L., Silman, M., and Morel, A.: Benchmark map of forest carbon stocks in tropical regions across three continents, Proc. Natl. Acad. Sci. USA, 108, 9899–9904, 2011. 4246

Sacks, W. J., Schimel, D. S., Monson, R. K., and Braswell, B. H.: Model-data synthesis of diurnal and seasonal CO_2 fluxes at Niwot Ridge, Glob. Change Biol., 12, 240–259, 2006. 4245

Saito, M., Maksyutov, S., Hirata, R., and Richardson, A. D.: An empirical model simulating diurnal and seasonal CO_2 flux for diverse vegetation types and climate conditions, Biogeosciences, 6, 585–599, doi:10.5194/bg-6-585-2009, 2009. 4261

Saito, M., Ito, A., and Maksyutov, S.: Evaluation of biases in JRA-25/JCDAS precipitation and their impact on the global terrestrial carbon balance, J. Climate, 24, 4109–4125, 2011. 4247

Sato, H., Itoh, A., and Kohyama, T.: SEIB-DGVM: a new Dynamic Global Vegetation Model using a spatially explicit individual-based approach, Ecol. Model., 200, 279–307, 2007. 4245

Schimel, D. S.: Terrestrial ecosystems and the carbon cycle, Glob. Change Biol., 1, 77–91, 1995. 4244

Scholze, M., Kaminski, T., Rayner, P., Knorr, W., and Giering, R.: Propagating uncertainty through prognostic carbon cycle data assimilation system simulations, J. Geophys. Res., 112, D17305, doi:10.1029/2007JD008642, 2007. 4246

GMDD
6, 4243–4280, 2013

Schubert, S. D., Rood, R. B., and Pfaendtner, J.: An assimilated dataset for earth science applications, B. Am. Meteorol. Soc., 74, 2331–2342, 1993. 4251
Scurlock, J. M. O., Cramer, W., Olson, R. J., Parton, W. J., and Prince, S. D.: Terrestrial NPP: toward a consistent data set for global model evaluation, Ecol. Appl., 9, 913–919, 1999. 4254
Sitch, S., Smith, B., Prentice, I. C., Arneth, A., Bondeau, A., Cramer, W., Kaplan, J. O., Levis, S., Lucht, W., Sykes, M. T., Thonicke, K., and Venevsky, S.: Evaluation of ecosystem dynamics, plant geography and terrestrial carbon cycling in the LPJ dynamic global vegetation model, Glob. Change Biol., 9, 161–185, 2003. 4245
Sitch, S., Huntingford, C., Gedney, N., Levy, P. E., Lomas, M., Piao, S. L., Betts, R., Ciais, P., Cox, P., Friedlingstein, P., Jones, C. D., Prentice, I. C., and Woodward, F. I.: Evaluation of the terrestrial carbon cycle, future plant geography and climate–carbon cycle feedbacks using five Dynamic Global Vegetation Models (DGVMs), Glob. Change Biol., 14, 2015–2039, 2008. 4245
Tans, P. P., Fung, I. Y., and Takahashi, T.: Observational contrains on the global atmospheric CO_2 budget, Science, 247, 1431–1438, 1990. 4244
Tarantola, A.: Inverse Problem Theory and Methods for Model Parameter Estimation, Society for Indstrial and Applied Mathematics, 2005. 4252
Thonicke, K., Spessa, A., Prentice, I. C., Harrison, S. P., Dong, L., and Carmona-Moreno, C.: The influence of vegetation, fire spread and fire behaviour on biomass burning and trace gas emissions: results from a process-based model, Biogeosciences, 7, 1991–2011, doi:10.5194/bg-7-1991-2010, 2010. 4260
Tjoelker, M. G., Oleksyn, J., and Reich, P. B.: Modelling respiration of vegetation: evidence for a general temperature-dependent Q_{10}, Glob. Change Biol., 7, 223–230, 2001. 4255
Valsala, V. and Maksyutov, S.: Simulation and assimilation of global ocean pCO_2 and air-sea CO_2 fluxes using ship observations of surface ocean pCO_2 in a simplified biogeochemical offline model, Tellus B, 62, 821–840, 2010. 4251
van der Werf, G. R., Morton, D. C., DeFries, R. S., Olivier, J. G. J., Kasibhatla, P. S., Jackson, R. B., Collatz, G. J., and Randerson, J. T.: CO_2 emissions from forest loss, Nat. Geosci., 2, 737–738, 2009. 4246
van Iersel, M. W.: Carbon use efficiency depends on growth respiration, maintenance respiration, and relative growth rate, a case study with lettuce, Plant Cell Environ., 26, 1441–1449, 2003. 4261

GMDD
6, 4243–4280, 2013

Wang, Y. P., Trudinger, C. M., and Enting, I. G.: A review of applications of model-data fusion to studies of terrestrial carbon fluxes at different scales, Agr. Forest Meteorol., 149, 1829–1842, 2009. 4245, 4261

Wright, I. J., Reich, P. B., Westoby, M., Ackerly, D. D., Baruch, Z., Bongers, F., Cavender-Bares, J., Chapin, T., Cornelissenohannes, J. H. C., Diemer, M., Flexas, J., Garnier, E., Groom, P. K., Gulias, J., Hikosaka, K., Lamont, B. B., Lee, T., Lee, W., Lusk, C., Midgley, J. J., Navas, M. L., Niinemets, U., Oleksyn, J., Osada, N., Poorter, H., Poot, P., Prior, L., Pyankov, V. I., Roumet, C., Thomas, S. C., Tjoelker, M. G., Veneklaas, E. J., and Villar, R.: The worldwide leaf economics spectrum, Nature, 428, 821–827, 2004. 4261

Zhao, M., Heinscha, F. A., Nemanib, R. R., and Running, S. W.: Improvements of the MODIS terrestrial gross and net primary production global data set, Remote Sens. Environ., 95, 164–176, 2005. 4261

Zhou, T. and Luo, Y.: Spatial patterns of ecosystem carbon residence time and NPP-driven carbon uptake in the conterminous United States, Global Biogeochem. Cy., 22, GB3032, doi:10.1029/2007GB002939, 2008. 4245

GMDD
6, 4243–4280, 2013

Table 1. List of VISIT prior parameters and their values.

Symbol	Parameter description (unit)	Prior	Scale
P_{max}	Potential maximum photosynthetic rate (μmol CO_2 $m^{-2}s^{-1}$)	1.5	$\times 10^{1}$
T_{min}	Minimum temperature for plant activities (°C)	−5.0	
T_{opt}	Optimum temperature for plant activities (°C)	2.5	$\times 10^{1}$
km_nstl	Photosynthesis limitation factor in terms of soil moisture	3.0	$\times 10^{-1}$
rg_{FL}	Specific growth respiration rate of leaf	3.5	$\times 10^{-1}$
rg_{RT}	Specific growth respiration rate of root	3.5	$\times 10^{-1}$
rm_{FL}	Specific maintenance respiration rate of leaf	1.0	
rm_{RT}	Specific maintenance respiration rate of root	4.0	$\times 10^{-1}$
Q_{10}	Temperature dependence of respiration rate	2.0	
lf_{FL}	Specific litter fall of leaf	2.4	$\times 10^{-4}$
lf_{SB}	Specific litter fall of stem	3.0	$\times 10^{-4}$
shl	Specific heterotrophic respiration rate at upper soil	2.0	
shm	Specific heterotrophic respiration rate at lower soil	8.0	$\times 10^{-1}$

GMDD
6, 4243–4280, 2013

Table 2. Mean values and standard deviations for AGB and NPP for each biome type.

Biome	AGB ($kg C m^{-2}$)		NPP ($g C m^{-2} yr^{-1}$)	
	IIASA	Posterior	GPPDI	Posterior
ENF	2.52 ± 1.01	2.07 ± 1.41	335 ± 186	419 ± 266
EBF	4.77 ± 3.79	4.85 ± 1.02	987 ± 180	1022 ± 188
DNF	2.23 ± 0.48	2.28 ± 1.58	322 ± 92	402 ± 138
DBF	4.35 ± 1.40	4.17 ± 1.93	522 ± 140	506 ± 215
MF	2.79 ± 1.25	2.34 ± 2.09	509 ± 235	421 ± 297
WL	3.35 ± 2.69	3.18 ± 2.26	550 ± 498	457 ± 310
WGL	1.40 ± 1.30	1.72 ± 1.15	502 ± 347	322 ± 297
CSL	0.13 ± 0.15	0.49 ± 0.42	–	–
TND	0.40 ± 0.52	0.20 ± 0.31	129 ± 117	58 ± 90
TOS	0.23 ± 0.51	0.35 ± 0.73	208 ± 345	100 ± 224
GL	0.46 ± 0.73	0.47 ± 0.36	369 ± 258	297 ± 195
CL	1.00 ± 1.01	0.84 ± 0.78	526 ± 269	392 ± 296
BG	0.00 ± 0.02	0.05 ± 0.06	255 ± 297	13 ± 21
WTL	1.27 ± 0.60	1.52 ± 0.72	–	–
SI	0.00 ± 0.03	0.02 ± 0.01	–	–

GMDD
6, 4243–4280, 2013

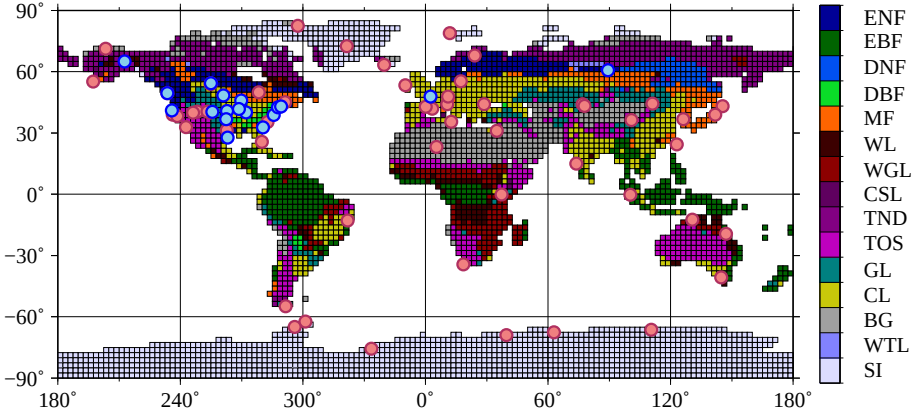

Fig. 1. Distributions of the dominant biomes in each grid and the locations of the atmospheric CO_2 observation sites. ENF: evergreen needle-leaf forest; EBF: evergreen broad-leaf forest; DNF: deciduous needle-leaf forest; DBF: deciduous broad-leaf forest; MF: mixed forest; WL: woodland; WGL: wooded grassland; CSL: closed shrubland; TND: tundra; TOS: temperate open shrubland; GL: grassland; CL: cropland; BG: bare ground; WTL: wetland; SI: snow and ice. The blue circles are partial column CO_2 concentrations and the red circles are surface CO_2 concentrations.

GMDD
6, 4243–4280, 2013

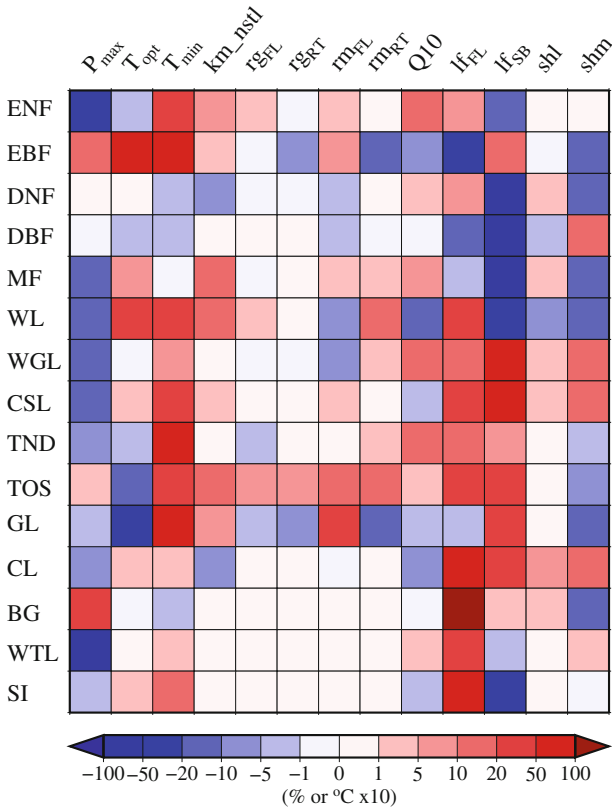

Fig. 2. Differences between the posterior parameters and the prior parameters expressed as fractions (%), except for the optimum temperature (T_{opt}) and minimum temperature (T_{min}), which are expressed as differences in °C scaled by 10.

GMDD
6, 4243–4280, 2013

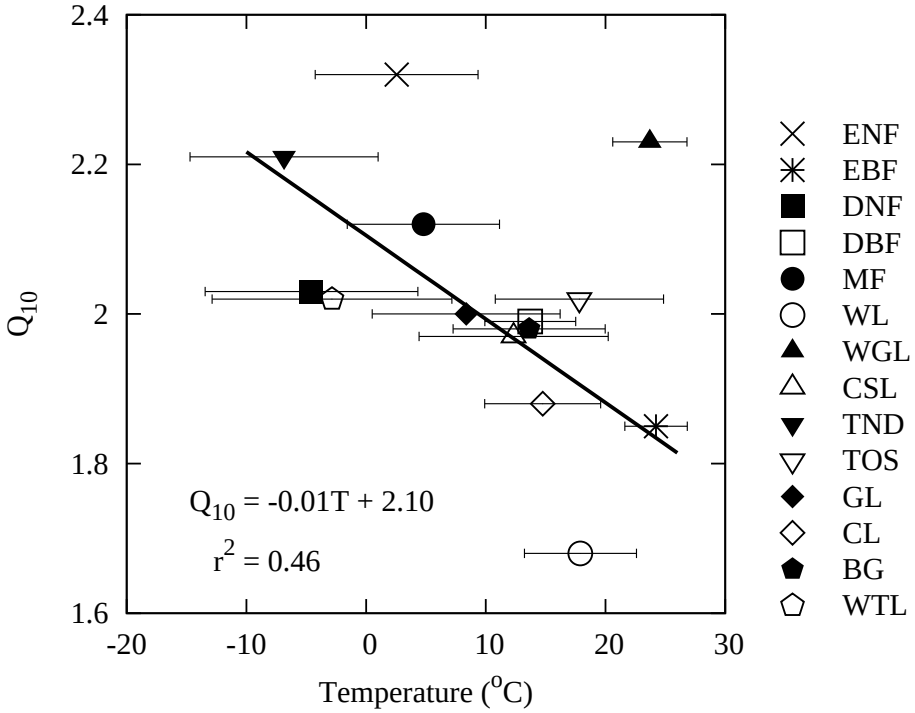

Fig. 3. Relationships between the mean annual temperature (°C) and posterior Q_{10} for each biome type, except for the snow and ice (SI) biome. Error bars are the standard deviations of the mean annual temperatures. The solid thick line is the linear regression fitted to all the data, except those for the wooded grassland (WGL) and SI.

GMDD
6, 4243–4280, 2013

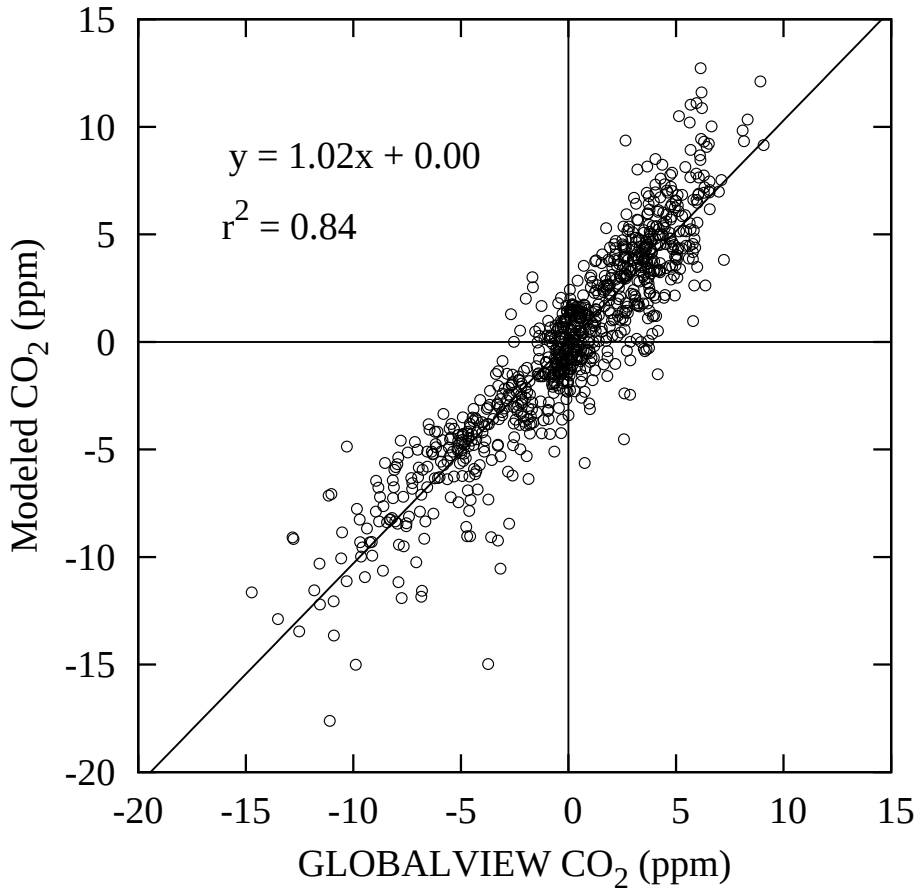

Fig. 4. Comparison of the mean monthly CO_2 variability calculated with GLOBALVIEW and with our model.

GMDD
6, 4243–4280, 2013

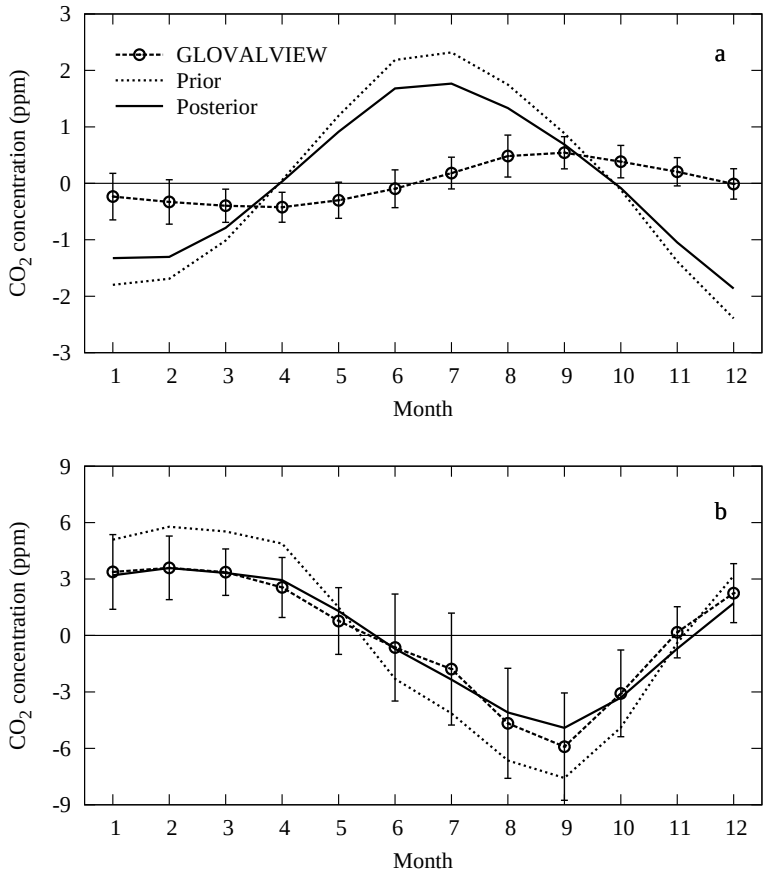

Fig. 5. Seasonal variations in the observed and modeled mean monthly CO_2 concentrations (ppm) at **(a)** Cape Grim station, Tasmania, Australia, and **(b)** Wendover station, Utah, USA. Open circles with the dashed lines are GLOBALVIEW-CO_2 data; the dotted lines represent the prior parameters; and the solid line represents the posterior parameters. The error bars indicate the uncertainties of the observations.

GMDD
6, 4243–4280, 2013

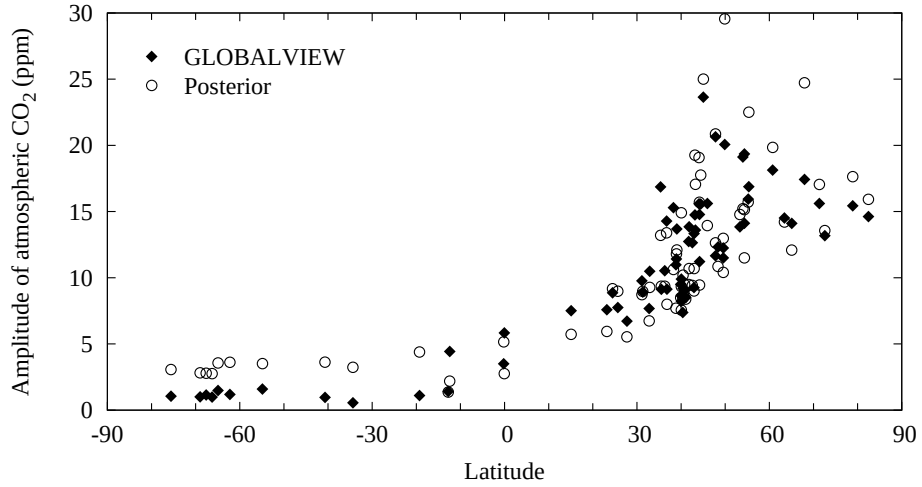

Fig. 6. Annual amplitudes of the atmospheric CO_2 variables (ppm) along specific latitudes. The closed diamonds represent the GLOBALVIEW-CO_2 data and the open circles represent the posterior parameters.

GMDD
6, 4243–4280, 2013

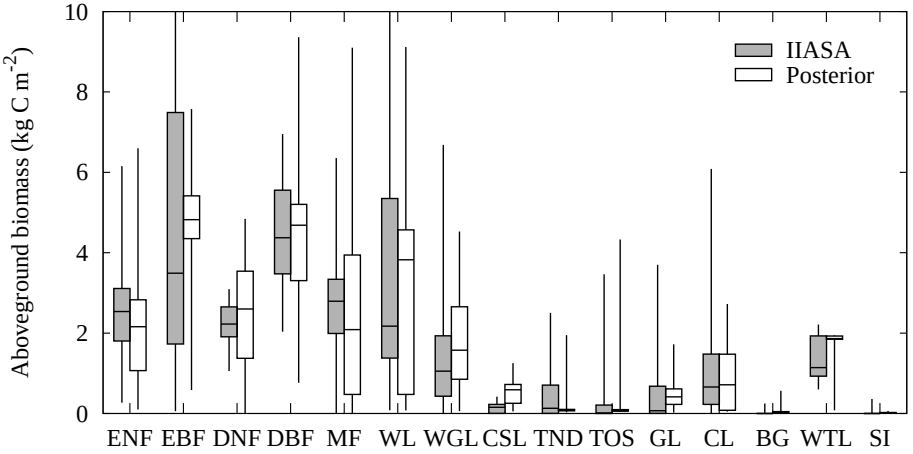

Fig. 7. Comparison of the aboveground biomass for each biome according to IIASA (gray box) and VISIT with posterior parameters (open box). The box-and-whisker plots show the median, the upper and lower quartiles, and the maximum and minimum data. The maximum aboveground biomass of the evergreen needle-leaf forest and woodland in IIASA reached 17.5 and 10.9 $kg C m^{-2}$, respectively.

GMDD
6, 4243–4280, 2013

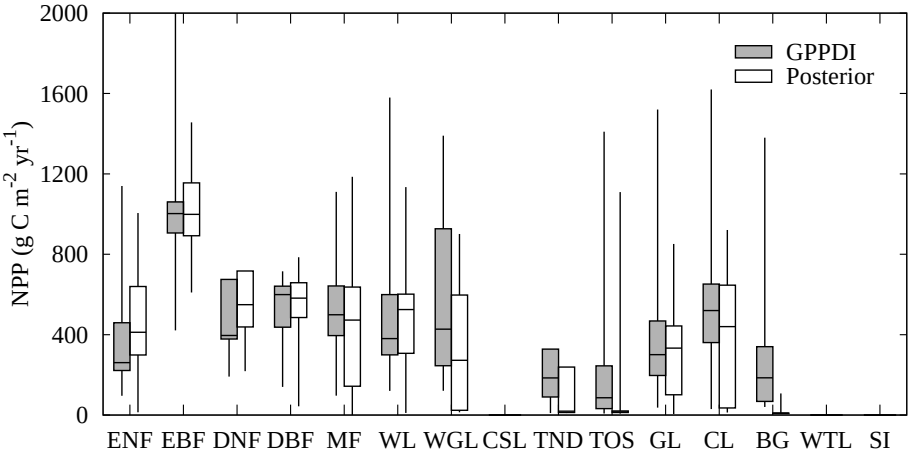

Fig. 8. As Fig. 7, except that NPP is compared between GPPDI and VISIT with posterior parameters. GPPDI does not contain NPP data in the grids corresponding to closed shrubland (CSL), wetland (WTL), or snow and ice (SI).

GMDD
6, 4243–4280, 2013